Nuclear Engineering and Technology 55 (2023) 3121–3125

Contents lists available at ScienceDirect

Nuclear Engineering and Technology

journal homepage: www.elsevier.com/locate/net

Original Article

Structural and component characterization of the B_4C neutron conversion layer deposited by magnetron sputtering

Jingtao Zhu [a], Yang Liu [a, b], Jianrong Zhou [b, c, *], Zehua Yang [d], Hangyu Zhu [a, b], Xiaojuan Zhou [b, c], Jinhao Tan [b, c], Mingqi Cui [c], Zhijia Sun [b, c, **]

[a] Key Laboratory of Advanced Micro-structured Materials, Ministry of Education, School of Physical and Engineering, Tongji University, Shanghai, 200092, China
[b] Spallation Neutron Source Science Center, Dongguan, 523803, Guangdong, China
[c] State Key Laboratory of Particle Detection and Electronics, Institute of High Energy Physics, Chinese Academy of Sciences, Beijing, 100049, China
[d] State Key Laboratory of Surface Physics, Department of Physics, Fudan University, Shanghai, 200438, China

ARTICLE INFO

Article history:
Received 22 March 2023
Received in revised form
1 May 2023
Accepted 9 May 2023
Available online 22 May 2023

Keywords:
Neutron conversion layer
Boron carbide film
Magnetron sputtering
X-ray photoelectron spectroscopy
Time-of-flight secondary ion mass spectrometry

ABSTRACT

Neutron conversion detectors that use ^{10}B-enriched boron carbide are feasible alternatives to ^{3}He-based detectors. We prepared boron carbide films at micron-scale thickness using direct-current magnetron sputtering. The structural characteristics of natural B_4C films, including density, roughness, crystallization, and purity, were analyzed using grazing incidence X-ray reflectivity, X-ray diffraction, X-ray photoelectron spectroscopy, time-of-flight secondary ion mass spectrometry, and scanning electron microscopy. A beam profile test was conducted to verify the practicality of the ^{10}B-enriched B_4C neutron conversion layer. A clear profile indicated the high quality of the neutron conversion of the boron carbide layer.

1. Introduction

Neutron detectors are important components in neutron experiments for monitoring flux. They are stable, highly sensitive, and have excellent neutron discrimination, ^{3}He-gas tube detectors are the product of radioactive decay from nuclear weapons and were widely used in the past [1,2]. However, in recent years, the supply of ^{3}He has decreased, resulting in the higher purchasing costs [3]. ^{10}B-based detectors are a viable alternative in terms of performance and economy [4–6]. ^{10}B has relatively high neutron absorption cross-section-3866 b for thermal neutrons (0.025 eV), which can reach 72% of the ^{3}He [7]. As an ideal ^{3}He substitute material, ^{10}B collides with thermal neutrons to produce the following two reactions:

$$^{10}B + n_{th}(0.025eV) \rightarrow {}^{4}He^{2+} + {}^{7}Li^{3+} + 2.31MeV + \gamma(0.48MeV) \quad (1)$$

$$^{10}B + n_{th}(0.025eV) \rightarrow {}^{4}He^{2+} + {}^{7}Li^{3+} + 2.79MeV \quad (2)$$

where the occurrence probabilities of Eqs. (1) and (2) are 94% and 6%, respectively. Through these two reactions, ^{10}B-contained materials absorb neutrons and produce high-energy charged particles. Secondary particles emitting in the opposite direction can escape out of the ^{10}B layer and ionize the detection gas of Ar and CO_2, which are collected by the electronic device as the detected signal. The neutron detection efficiency is the product of the efficiency of ^{10}B-layer absorbing neutrons and the probability of charged particles escaping from the ^{10}B layer.

Boron carbide film is the most common configuration of the ^{10}B-containing neutron conversion layer. In 2012, Hoglund et al. grew boron carbide films for neutron detection using direct-current (DC) magnetron sputtering with an industrial deposition system [8], high-quality boron carbide films were prepared by increasing the substrate temperature and sputtering rate. Schmidt et al.

* Corresponding author. Spallation Neutron Source Science Center, Dongguan, 523803, Guangdong, China.
** Corresponding author. Spallation Neutron Source Science Center, Dongguan, 523803, Guangdong, China.
E-mail addresses: zhoujr@ihep.ac.cn (J. Zhou), sunzj@ihep.ac.cn (Z. Sun).

https://doi.org/10.1016/j.net.2023.05.013

characterized the properties of boron carbide films prepared at different substrate temperatures and working pressures [9]. Pedersen et al. explored chemical vapor deposition methods to grow amorphous boron carbide films [10]. Nowak et al. explored the process of preparing neutron conversion layer films at room temperature [11]. In addition, DC magnetron sputtering was shown to provide high quality $^{10}B_4C$ neutron conversion layer for large-area neutron detectors [8,9,11–13].

With the building of the China Spallation Neutron Source (CSNS), a large number of neutron scattering spectrometers will be developed, which need highly efficient large-area position-sensitive detectors [14]. Therefore, it is important to explore the preparation process of the neutron conversion layer to meet the requirements for developing neutron detectors. In our study, we introduce the preparation of natural B_4C and ^{10}B-enriched B_4C films using a DC large-area magnetron sputtering boron coating device. The magnetron sputtering deposition technique was chosen for its high deposition rate, low impurities and high density of films. Natural B_4C samples were characterized by grazing incidence X-ray reflectivity (GIXRR), X-ray diffraction (XRD), X-ray photoelectron spectroscopy (XPS), time-of-flight secondary ion mass spectrometry (TOF-SIMS), and scanning electron microscopy (SEM). To verify the practicality of the ^{10}B-enriched B_4C neutron conversion layer, we also conducted a beam profile test.

2. Preparation and characterization

Natural and ^{10}B-enriched B_4C monolayer samples were deposited on silicon wafers, float glass, and aluminum substrates using a DC magnetron sputtering deposition system. The two rectangular targets (Ti and natural B_4C) used in the experiments had the same size (750 mm × 125 mm). The purity of the Ti target was 99.95% and that of the B_4C target was 99.5%. Sputtering power for both targets was set to 1000 W. The round ^{10}B-enriched B_4C target ($^{10}B \geq 95\%$) had a diameter of 4 inches with 200 W of sputtering power. All the samples were fabricated at residual gas atmosphere pressure below 2×10^{-4} Pa. Ar gas (99.999% purity) was used as sputtering gas at 0.5 Pa pressure. The thickness of sample was precisely controlled using a servomotor to adjust the moving speed and repetition times of the sample holder in the sputtering area.

GIXRR and XRD measurements were performed using an X-ray diffractometer (PANalytical Empyrean, Netherlands) equipped with a Cu target to import a Cu K_α-line (0.154 nm). The measured GIXRR curves were fitted using Parratt's recursive formula [15] to obtain the average thickness, density, and interfacial width of multilayers from the model. XPS measurements were conducted on a Thermo Fisher Scientific Nexsa with a 1.48 keV X-ray source of monochromatic Al-K_α radiation. TOF-SIMS experiments were carried out on an ION-TOF SIMS 5 with sputtered ions of O^{2+} at 1 KeV. The SEM instrument was a ZEISS Sigma 300 with a secondary electron detector operating at an accelerating voltage of 3.0 kV and a working distance of 6.1 mm.

3. Experiments and analysis

The GIXRR measurement was conducted to calibrate the deposition rate of B_4C films. A natural B_4C monolayer was coated on a float glass substrate (75 mm × 25 mm × 1.2 mm). The Ti interlayer was pre-coated in order to increase the adhesion of the film. Fig. 1 shows the GIXRR measurements (black circles) and the corresponding fitting results (red curve). We can see clear interference modulation on the reflective intensity, indicating the continuous layers of the film. The fitting data indicate that the Ti layer and B_4C layer are 6.7 nm and 40.6 nm thick, respectively. The density of the B_4C layer is 2.37 g/cm^3 (94% of the bulk value), and the fitting interfacial roughness is 1.0 nm.

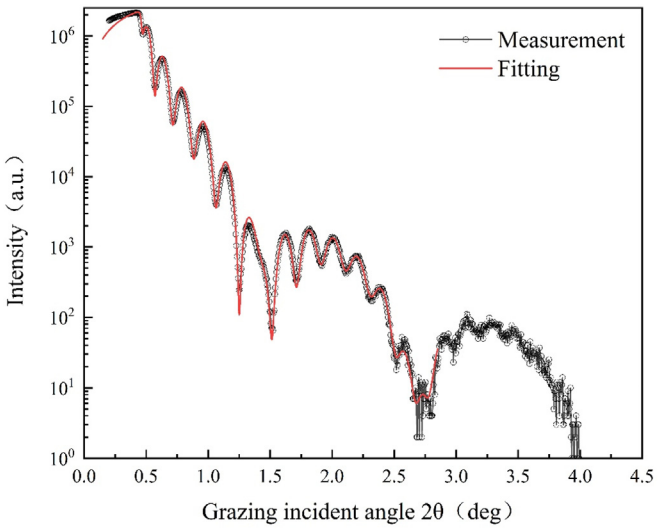

Fig. 1. GIXRR measurements of the B_4C film with a Ti adhesion layer. The red curve shows the fitting results. (For interpretation of the references to colour in this figure legend, the reader is referred to the Web version of this article.)

Crystalline phase analysis was characterized by XRD. A 1.5 μm natural B_4C monolayer was deposited on a 75 mm × 25 mm × 2.5 mm aluminum substrate. The XRD measurement results are shown in Fig. 2, showing clear peaks at 38.4°8 44.7°, 65.2°5 78.3°, identified as characteristic peaks of Al (111), (200), (220), and (311), respectively, without the characteristic peak of boron carbide. Thus, the B_4C film is amorphous.

To characterize the impurity concentrations of the film, a 500 nm natural B_4C monolayer was deposited on the Si substrate for XPS measurements. The depth distribution of the chemical composition for this sample is shown in Fig. 3. The atomic concentration at different depths of the film is expressed as a function of the etching time, which is equivalent to the etching depth. Avantage software was used to calculate the content or relative concentration of atoms at each analysis point. In Fig. 3, the impurity concentrations of O and N are 10 at.% and 1 at.%, respectively, located in a normal range. The stoichiometric ratio of boron and

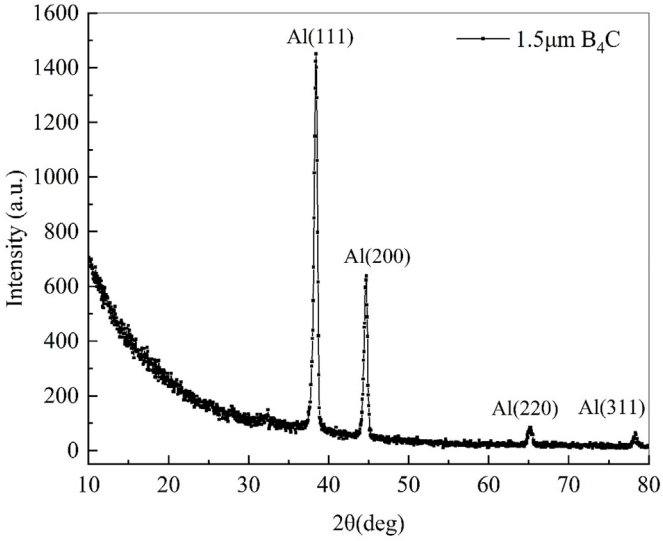

Fig. 2. XRD curve of B_4C film coated on an Al substrate.

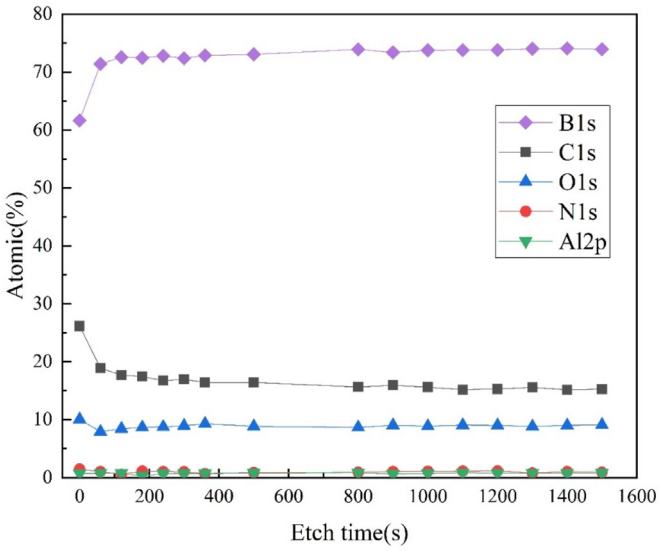

Fig. 3. XPS depth profiles for the 500 nm B_4C film.

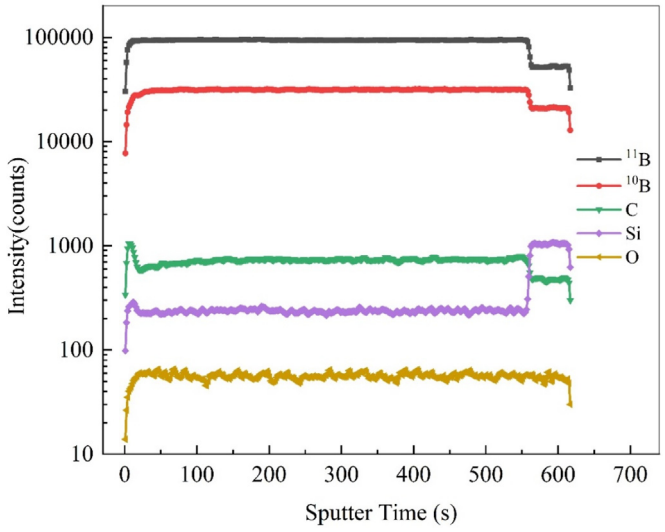

Fig. 4. TOF-SIMS depth profiles for the 500 nm B_4C film.

carbon atoms (B/C) is 4.72 higher than that of natural boron carbide. This is attributed to the loss of C atoms from the re-sputtering effect [16]. The signal intensity of each element fluctuates little after 100 s, indicating that each element is evenly distributed over the entire depth range of the layer. We also performed a depth profile analysis of the sample using TOF-SIMS to determine the content of ^{10}B. Fig. 4 presents the results of the TOF-SIMS measurements of ^{10}B, ^{11}B, Ti, C, Si, and O. The signal intensity of Si increased suddenly after 550 s of etching, indicating that the B_4C film was penetrated at this time. The percentage of ^{11}B and ^{10}B in the boron element in the sample is 76.7% and 23.3%, respectively, with a ratio of 3.3, which is close to the isotopic ratio in natural boron ($^{11}B/^{10}B = 4.02$). However, the higher B/C and lower $^{11}B/^{10}B$ indicate increasing ^{10}B content in the film, which can improve the efficiency of neutron detection.

To determine the nanostructure of the B_4C films during their growth, we also prepared a 2.3 μm natural B_4C monolayer on a Si substrate. A 10 nm Ti layer was pre-coated to increase the adhesion of the Si substrate. Fig. 5 shows a cross-sectional image of the sample measured by scanning electron microscopy. The mechanical fracture of the cross-section of the B_4C film is clearly visible in Fig. 5(b). The columnar structure has no cracks or voids, indicating the high uniformity and compactness of the sample.

To verify the practical performance of the boron carbide neutron conversion layer, we conducted a beam profile test at the BL20, CSNS. A 1 μm ^{10}B-enriched B_4C layer was deposited onto a 0.2 mm aluminum substrate as the cathode for a ceramic gas electrons multiplier (GEM) neutron detector [17]. The schematic diagram of the ceramic GEM neutron detector was shown in Fig. 6(a). The incident neutron was captured by ^{10}B and converted to charged particles, which may enter the drift region and produce primary ionization. Then, the generated electrons were multiplied by the ceramic GEM. Fig. 6(b) shows the configuration of the detector. It was filled with a mixture of Ar and CO_2 (90%:10%) and adjusted to be perpendicular to the neutron beam aligned by a laser collimator. A cadmium plate was placed between the detector and the neutron beam to change the profile of the neutron imaging. For the strong absorption properties of cadmium to thermal neutrons, only the aperture of the cadmium plate can allow neutrons to enter the detector. Fig. 7 shows the measured beam profile and the corresponding one-dimensional distributions. The circular spot has the diameter of approximately 25 mm, with a clear boundary. Due to fluctuations in the intensity of the neutron beam, the collected counting points fluctuate slightly in Fig. 7(a). The one-dimensional distributions were obtained by projecting the beam profile in the direction of two coordinate axes, shown in Fig. 7(b) and (c). The results demonstrate that the boron carbide neutron conversion layer can be applied to practical neutron detection.

4. Conclusion

We prepared a series of micron-scale B_4C films using magnetron

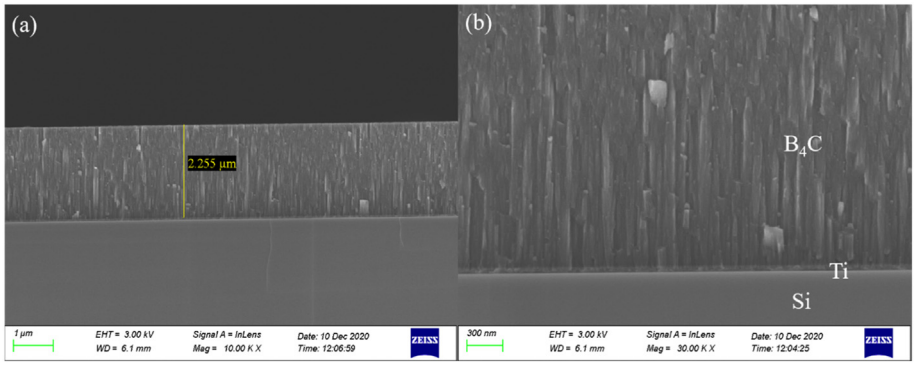

Fig. 5. SEM cross-section of a 2.3 μm B_4C film at (a) 10,000 × and (b) 30,000 × magnification.

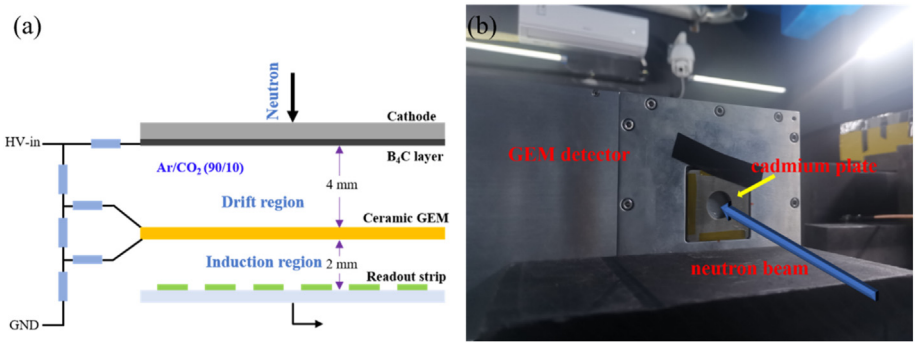

Fig. 6. The schematic diagram(a) and configuration(b) of the ceramic GEM neutron detector.

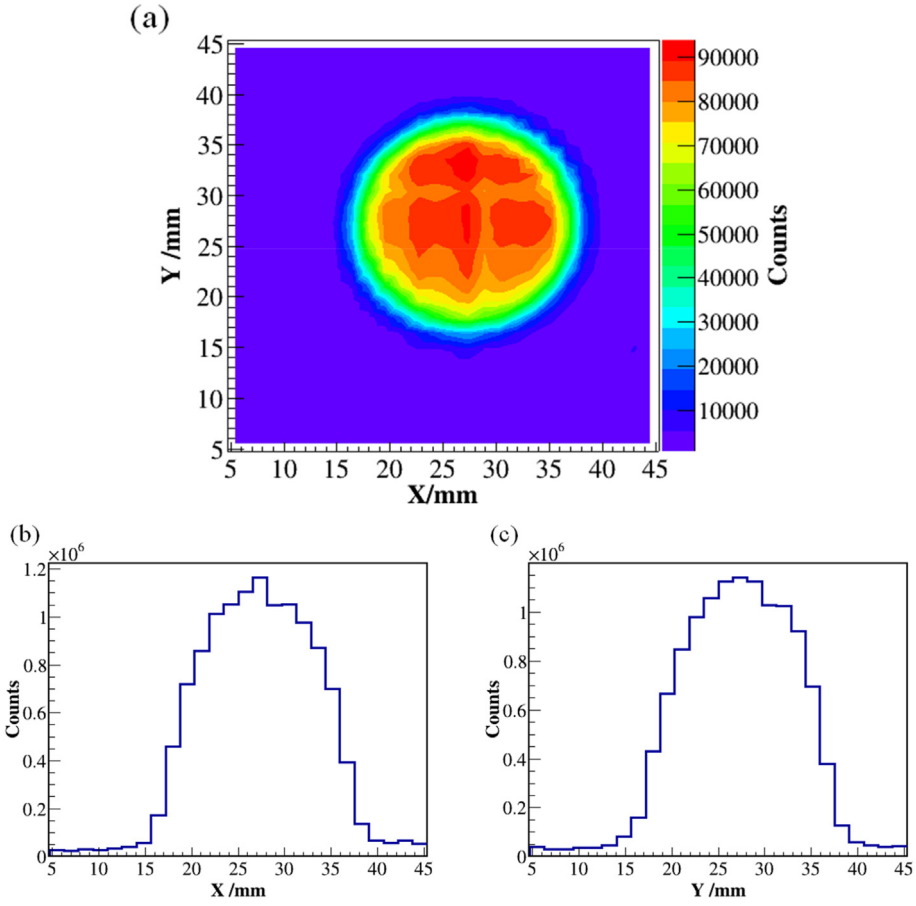

Fig. 7. Image (a) and one-dimensional distributions in the *x* (b) and *y* (c) directions of the beam profile.

sputtering as neutron conversion layers. The GIXRR and XRD measurements demonstrated the high quality, precise thickness, and amorphous formation of the natural B_4C films. The XPS and TOF-SIMS depth profiles showed that the stoichiometric ratio between boron and carbon atoms (B/C) was 4.72, while the impurity concentrations were O of 10 at.% and N of 1 at.%. The ratio of the two isotopes ($^{11}B/^{10}B$) was 3.3, close to that of natural boron carbide. Each element distributed evenly over the entire depth range of the layer. Cross-sectional SEM images showed the high uniformity and compactness of the natural B_4C films during their growth. A beam profile test of the ^{10}B-enriched B_4C layer obtained a clear circular spot from neutron imaging, confirming the feasibility of the boron carbide neutron conversion layers assembled in a neutron detector for neutron detection.

Declaration of competing interest

The authors declare that they have no known competing financial interests or personal relationships that could have appeared to influence the work reported in this paper.

Acknowledgments

This work was supported by the National Natural Science Foundation of China (Grant Nos. U1932167, 12175254, 11875204, 12227810, U2032166, 11975255), and Fundamental Research Funds for the Central Universities (22120210446 and 22120180070).

References

[1] Z. Zhang, Y. Liang, W. Li, Z. Wang, H. Chen, Stress evolution in B4C and Cr mono-layer and B4C/Cr multilayer films with variable layer thickness for neutron detectors, Thin Solid Films 531 (2013) 302–305, https://doi.org/10.1016/j.tsf.2013.01.084.

[2] J.L. Lacy, A. Athanasiades, L. Sun, C.S. Martin, T.D. Lyons, M.A. Foss, H.B. Haygood, Boron-coated straws as a replacement for 3He-based neutron detectors, Nucl. Instruments Methods Phys. Res. Sect. A Accel. Spectrometers, Detect. Assoc. Equip. 652 (2011) 359–363, https://doi.org/10.1016/j.nima.2010.09.011.

[3] A. Cho, Helium-3 shortage could put freeze on low-temperature Research, Science 326 (2009) 778–779, https://doi.org/10.1126/science.326_778.

[4] K. Zeitelhack, Search for alternative techniques to helium-3 based detectors for neutron scattering applications, Neutron News 23 (2012) 10–13, https://doi.org/10.1080/10448632.2012.725325.

[5] F. Piscitelli, A. Khaplanov, A. Devishvili, S. Schmidt, C. Höglund, J. Birch, A.J.C. Dennison, P. Gutfreund, R. Hall-Wilton, P. Van Esch, Neutron reflectometry on highly absorbing films and its application to (B4C)-B-10-based neutron detectors, Proc. R. Soc. A-Math. Phys. Eng. Sci. 472 (2016), https://doi.org/10.1098/rspa.2015.0711.

[6] M. Henske, M. Klein, M. Köhli, P. Lennert, G. Modzel, C.J. Schmidt, U. Schmidt, The 10B based Jalousie neutron detector – an alternative for 3He filled position sensitive counter tubes, Nucl. Instruments Methods Phys. Res. Sect. A Accel. Spectrometers, Detect. Assoc. Equip. 686 (2012) 151–155, https://doi.org/10.1016/j.nima.2012.05.075.

[7] N. Hong, An Exploration of Neutron Detection in Semiconducting Boron Carbide, The University of Nebraska, Lincoln, 2012.

[8] C. Höglund, J. Birch, K. Andersen, T. Bigault, J.-C. Buffet, J. Correa, P. van Esch, B. Guerard, R. Hall-Wilton, J. Jensen, A. Khaplanov, F. Piscitelli, C. Vettier, W. Vollenberg, L. Hultman, B4C thin films for neutron detection, J. Appl. Phys. 111 (2012), https://doi.org/10.1063/1.4718573.

[9] S. Schmidt, C. Höglund, J. Jensen, L. Hultman, J. Birch, R. Hall-Wilton, Low-temperature growth of boron carbide coatings by direct current magnetron sputtering and high-power impulse magnetron sputtering, J. Mater. Sci. 51 (2016) 10418–10428, https://doi.org/10.1007/s10853-016-0262-4.

[10] H. Pedersen, C. Höglund, J. Birch, J. Jensen, A. Henry, Low temperature CVD of thin, amorphous boron-carbon films for neutron detectors, Chem. Vap. Depos. 18 (2012) 221–224, https://doi.org/10.1002/cvde.201206980.

[11] G. Nowak, M. Störmer, H.W. Becker, C. Horstmann, R. Kampmann, D. Höche, M. Haese-Seiller, J.F. Moulin, M. Pomm, C. Randau, U. Lorenz, R. Hall-Wilton, M. Müller, A. Schreyer, Boron carbide coatings for neutron detection probed by x-rays, ions, and neutrons to determine thin film quality, J. Appl. Phys. 117 (2015), https://doi.org/10.1063/1.4905716.

[12] T. Bigault, J. Birch, J.C. Buffet, J. Correa, R. Hall-Wilton, L. Hultman, C. Höglund, B. Guérard, A. Khaplanov, F. Piscitelli, P. Van Esch, 10B multi-grid proportional gas counters for large area thermal neutron detectors, Neutron News 23 (4) (2012) 20–25, https://doi.org/10.1080/10448632.2012.725329.

[13] I. Stefanescu, Y. Abdullahi, J. Birch, I. Defendi, R. Hall-Wilton, C. Höglund, L. Hultman, D. Seiler, K. Zeitelhack, Development of a novel macrostructured cathode for large-area neutron detectors based on the 10B-containing solid converter, Nucl. Instruments Methods Phys. Res. Sect. A Accel. Spectrometers, Detect. Assoc. Equip. 727 (2013) 109–125, https://doi.org/10.1016/j.nima.2013.06.003.

[14] H. Chen, X.L. Wang, China's first pulsed neutron source, Nat. Mater. 15 (2016) 689–691, https://doi.org/10.1038/nmat4655.

[15] L.G. Parratt, Surface studies of solids by total reflection of X-rays, Phys. Rev. 95 (1954) 359–369, https://doi.org/10.1103/PhysRev.95.359.

[16] M.-L. Wu, J.D. Kiely, T. Klemmer, Y.-T. Hsia, K. Howard, Process–property relationship of boron carbide thin films by magnetron sputtering, Thin Solid Films 449 (2004) 120–124, https://doi.org/10.1016/S0040-6090(03)01464-0.

[17] J. Zhou, X. Zhou, J. Zhou, X. Jiang, J. Yang, L. Zhu, W. Yang, T. Yang, H. Xu, Y. Xia, G.-a. Yang, Y. Xie, C. Huang, B. Hu, Z. Sun, Y. Chen, A novel ceramic GEM used for neutron detection, Nucl. Eng. Technol. 52 (2020) 1277–1281, https://doi.org/10.1016/j.net.2019.11.021.